Parametric control of microstructures in directional solidification

Pierre Pelce and Daniel Rochwerger
Laboratoire de Recherche en Combustion, Université de Provence-St. Jerome, Case 252, 13397 Marseille CEDEX 13, France
(Received 18 February 1992)

We consider the effect of a periodic oscillation on the growth velocity of a liquid-solid interface during the directional solidification of a binary mixture. By using a different formalism for the description of the interface motion, we confirm the eventual stabilizing properties of the oscillation found in the analysis of Wheeler [J. Cryst. Growth **67**, 8 (1984)] in the same configuration. In addition, we determine, in the small-forcing-parameter limit, the regions in the stability diagram where the oscillation has a stabilizing or a destabilizing effect. A stabilizing effect is found in an intermediate range of wave numbers and for a frequency larger than unity. The stabilizing effect is increased for larger partition coefficient and larger forcing frequencies. The magnitude of the capillary length is relatively neutral concerning this stabilization.

PACS number(s): 68.70.+w, 81.10.Fq

INTRODUCTION

Directional solidification of melts is a major problem of metallurgy. Depending on the conditions of growth, microstructures form on the solidifying liquid-solid interface and determine the mechanical properties of the material. A method frequently used for the solidification of gas-turbine blades is directional casting where the crystal develops from a chill [1]. The inconvenience of the method is that the microstructure which develops on the solidifying interface is not uniform because growth rate and temperature gradient cannot be controlled during the growth. More refined is the Bridgman-type method which allows one to grow crystals at constant velocity in a uniform temperature gradient [1]. The analysis of the microstructures of the solidifying interface which develop in this configuration was studied extensively during the past ten years on model systems like the binary mixture succinonitrile-acetone [2]. For a fixed temperature gradient the flat interface is stable at low velocity. Above a critical velocity the interface becomes cellular with a well-defined primary spacing function of the pulling velocity. Above a second larger critical velocity, the cells become dendritic and their primary spacing less homogeneous [3]. Then for larger velocity the flat interface restabilizes. Thus for a directional growth at constant velocity: Microstructures appear inevitably in a large domain of the control parameters; and microstructures cannot be controlled, i.e. for given temperature gradient and growth velocity, morphologies and primary spacing are determined after a nonlinear nonsteady growth, where intrinsic nonlinearities or extrinsic noise can affect the characteristics of the final state of the microstructure.

The basic idea that we begin to investigate in that paper is that if, on the constant control parameters mentioned previously, we superpose an adequate time-dependent component, the range of control parameters where microstructures appear can be either reduced or extended. And microstructures can be controlled, morphologies as well as primary spacing.

This idea was inspired from an experiment on flame propagation in a tube. When a cellular flame reaches some particular position in the tube, the acoustic energy contained in the tube suddenly increases and the flame oscillates in the acoustic field so generated [4]. At the same time, the cellular structure disappears and the flame can propagate with a flat shape even if its burning velocity is well above the critical velocity characterizing the cellular instability of flames propagating at constant velocity. This property was explained by Markstein [5] and implemented by Searby and Rochwerger [6] by showing that a disturbance of the shape of a flat flame oscillating in a periodic acoustic field satisfies a Mathieu equation.

In the case of directional solidification of binary alloys, Wheeler [7] showed that the effect of a periodic growth rate on a solidifying planar liquid-solid interface was in general stabilizing. A simple way to make the liquid-solid interface oscillate is to add an oscillatory component to the pulling velocity of the sample. Another equivalent way, which will be adopted in the analysis, is to add in phase an oscillatory component to the temperature of the heaters which maintain the temperature gradient. In that case, a point of constant temperature moves relatively to the heaters with an oscillating velocity.

We consider here a planar liquid-solid interface in such a moving temperature gradient and reconsider the analysis of Wheeler [7] by using an integro-differential equation for the solidifying interface. We first describe the motion of the planar liquid-solid interface when the oscillating component of an isotherm velocity is a sinusoidal function. Then we study the stability of this interface and confirm the results found by Wheeler, i.e., that a flat oscillating interface can remain stable versus shape deformations even if the control parameters of the directional solidification are in the instability range of the growth at constant parameters. In addition to this analysis, in order to investigate the stability property more carefully, we perform an analytical expansion of the growth rate of a perturbation at small forcing parameter

and delimit, in the stability diagram of the growth at constant velocity, regions where the growth rate is lowered or increased by the oscillating component. We study the relative size of these regions as a function of the material properties (partition coefficient, capillary length) and of the frequency of the oscillation.

I. MODEL

In directional solidification of a binary liquid mixture, the motion of the solidification front is determined by the diffusion of solute in the melt together with a set of boundary conditions on the interface. The solute concentration c satisfies the usual diffusion equation

$$\frac{\partial c}{\partial t}=D\Delta c \tag{1}$$

in the liquid and diffusion in the solid is neglected. Temperature and solute concentration at the interface are related by the local interfacial curvature by the Gibbs-Thomson relation

$$T=T_0+mc-\frac{\sigma T_0}{QR}\ . \tag{2}$$

Here, D is the coefficient of solute diffusivity in the liquid, m the slope of the liquidus line in the binary phase diagram, T_0 the crystallization temperature of the pure melt, R the local radius of curvature, Q the latent heat released per unit volume, and σ the liquid-solid surface tension. As, in the slow growth regime, the latent heat release at the interface can be neglected, the temperature in the sample is simply $T=T_p+G(z-f(t))$. Here $T_p=T_0+mc_\infty/K$ is the temperature of the planar interface and $f(t)=\int^t v(t')dt'$ is the time-dependent position of the isotherm at temperature T_p. G is the temperature gradient imposed on the sample, K the partition coefficient, and c_∞ the bulk mixture composition. In addition, solute conservation at the interface requires

$$c(1-K)\mathbf{v}\cdot\mathbf{n}=-D\nabla c\cdot\mathbf{n}\ . \tag{3}$$

In the following, we use dimensionless quantities defined as $u=K(c-c_\infty)/c_\infty(1-K)$ for the concentration field and $1/2\nu=D/U_0 l_T$ for the control parameter of the growth. Here, U_0 is the constant velocity of the liquid-solid interface when the oscillating component of the heaters is switched off and l_T the thermal length defined as $l_T=|m|c_\infty(1-K)/K$. Green-function method allows one to determine an integro-differential equation for the shape of the interface as (see Appendix A)

$$\begin{aligned}\frac{1}{2}\left[2-\frac{d_0}{R}-\frac{1}{2\nu}[z(x,t)-f(t)]\right]&=+\int_{-\infty}^{t}dt'\int_{-\infty}^{+\infty}dx'[1+\dot z(x',t')]\left[1+K\left[\frac{d_0}{R'}+\frac{1}{2\nu}[z(x',t')-f(t')]\right]\right]G(p,p')\\&\quad-\int_{-\infty}^{t}dt'\int_{-\infty}^{+\infty}dx'\left[\frac{d_0}{R'}+\frac{1}{2\nu}[z(x',t')-f(t')]\right]\left[\frac{\partial G}{\partial z'}(p,p')-\frac{\partial z}{\partial x'}\frac{\partial G}{\partial x'}(p,p')\right]\end{aligned} \tag{4}$$

where

$$G(p|p')=\frac{Y(t-t')}{4\pi(t-t')}\exp\left[-\frac{(x-x')^2+(z-z'+t-t')^2}{4(t-t')}\right] \tag{5}$$

is the Green function of the diffusive field in a frame moving with constant unit velocity, and p [p'] the points of coordinates (x,z,t) [(x',z',t')]. Here, length is adimensionalized by the diffusive length D/U_0, velocity by U_0 and time by D/U_0^2.

II. FLAT OSCILLATING INTERFACE

Consider that the temperatures of the heaters which maintain the temperature gradient oscillate in phase with a sinusoidal component, $T=T_{st}+\Delta T\sin\Omega t$. Then, the flat interface oscillates in the temperature gradient moving with the velocity $v=(\Delta T\Omega\cos\Omega t/G)$. [The corresponding isotherm position is $f(t)=f_0\sin\Omega t$ where $f_0=\Delta T/G$.] From Eqs. (4) and (5), one deduces an integro-differential equation for the interface position $z_0(t)$:

$$\begin{aligned}1-\frac{1}{4\nu}[z_0(t)-f(t)]&=\int_{-\infty}^{t}dt'\frac{1}{\sqrt{4\pi(t-t')}}\exp\left[-\frac{[z_0(t)-z_0(t')+t-t']^2}{4(t-t')}\right][(1+\dot z_0(t')]\left[1+\frac{K}{2\nu}[z_0(t')-f(t')]\right]\\&\quad-\frac{1}{2}\frac{[z_0(t')-f(t')]}{2\nu}\left[1+\frac{[z_0(t)-z_0(t')]}{(t-t')}\right].\end{aligned} \tag{6}$$

To integrate Eq. (6) numerically, one proceeds as follows: One discretizes the interval $]-\infty,t[$ with N points located at $t_i=t-i\Delta t$, $i=1$ to N. the product $N\Delta t$ is sufficiently large in order that the integral evaluated on the segment $[t_N,t]$ by using the trapezoidal rule approximates correctly the whole integral. Suppose known the values $z_i=z_0(t_i),i=1$ to N, one determines the value $z_0(t)$ by using the secant method on the difference between the left-hand side (lhs) and right-hand side (rhs) of Eq. (6). As an initial condition ($t=0$), one chooses $z_0=0$ for $t\leq 0$ and the forcing term $f(t)$ is applied for $t\geq 0$.

For given parameters, K,ν,f_0,Ω one determines z_0 as a function of time as is shown in Fig. 1. After a transient stage, the interface oscillates with a well-defined period T in the temperature gradient. A useful quantity characterizing this oscillation is the mean position of the interface:

$$\bar{z}_0=\frac{1}{T}\int_0^T z_0(t)dt \ . \tag{7}$$

An important property of the interface oscillation is that despite the fact that $f(t)$ has a zero mean value, $\bar{z}_0$ is positive, i.e., the mean position of the oscillating interface is displaced towards the liquid. It follows that the mean undercooling $\Delta=1-\bar{z}_0/2\nu$ is reduced with possible consequences on the stability of the flat oscillating liquid-solid interface [8]. In Fig. 2 we draw $\bar{z}_0$ as a function of Ω for $K=0.5$ and for $f_0=2$ and 4.

In order to understand more completely these curves, one can perform an analytical expansion of Eq. (6) at small forcing amplitude f_0. For this, one expands $z_0(t)$ as

$$z_0(t)=\frac{f_0}{2i}\alpha_1\exp(i\Omega t)-\frac{f_0}{2i}\alpha_1^*\exp(-i\Omega t)+\frac{f_0^2}{4}[\beta_2+\alpha_2\exp(2i\Omega t)+\alpha_2^*\exp(-2i\Omega T)] \ . \tag{8}$$

After identification of the terms of the expansion of same order in Eq. (6), one obtains

$$\alpha_1(\Omega)=\frac{1}{1-\dfrac{1+2i\Omega}{1-2\nu\dfrac{\sqrt{1+4i\Omega}}{1+\dfrac{2K-1}{\sqrt{1+4i\Omega}}}}} \tag{9}$$

and

$$K\frac{\beta_2}{2\nu}=-|\alpha_1|^2\left[\Omega\,\mathrm{Im}\frac{1}{\sqrt{1+4i\Omega}}+\left[\frac{1}{2}-\frac{(1-K)}{2\nu}\right]\left[2-\mathrm{Re}\sqrt{1+4i\Omega}-\mathrm{Re}\frac{1}{\sqrt{1+4i\Omega}}\right]\right]+\frac{K}{\nu}\Omega\,\mathrm{Im}\alpha_1-\frac{(1-K)}{2\nu}\mathrm{Re}\left[\alpha_1^*\left[\sqrt{1+4i\Omega}+\frac{1}{\sqrt{1+4i\Omega}}-2\right]\right] \ . \tag{10}$$

III. LINEAR STABILITY ANALYSIS OF THE FLAT OSCILLATING INTERFACE

Consider a slightly distributed planar interface $z=z_0(t)+z_1(t)\exp(ikx)$, where z_1, the amplitude of the disturbance, is much smaller than z_0. Then from Appendix B, z_1 satisfies

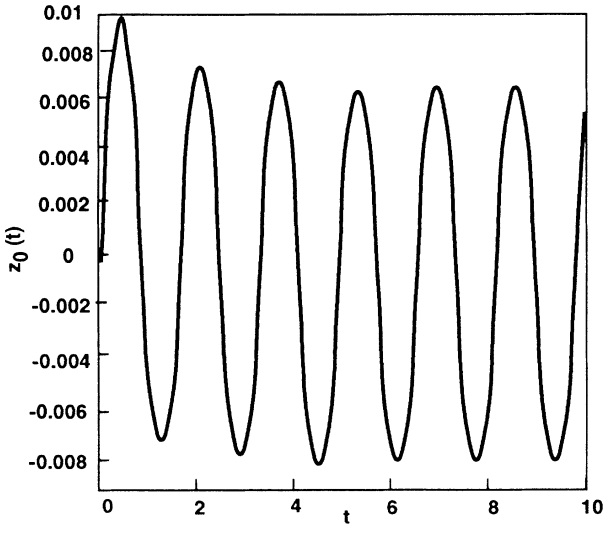

FIG. 1. Time evolution of the position of the planar interface under periodic forcing conditions. Here, $K=0.1$, $1/2\nu=0.5$, $\Omega=4$, and $f_0=0.025$.

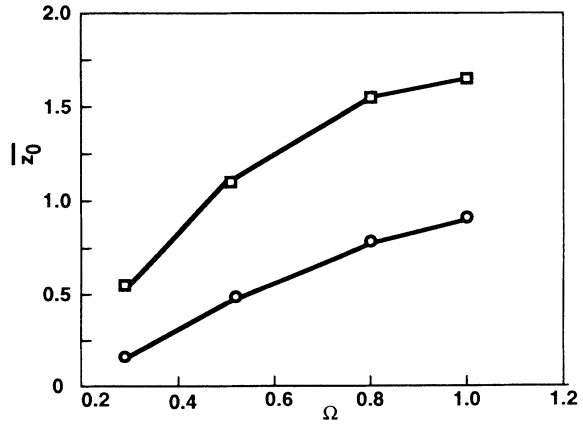

FIG. 2. Mean position of the liquid-solid interface as function of the forcing frequency. The material parameters are $d_0=0.01$, $K=0.5$. The control parameter of the growth is $1/2\nu=1.5$. The upper curve (white squares) corresponds to the forcing parameter $f_0=4$. The other one (black circles) to $f_0=2$.

$$z_1(t)A(t,k)=\int_{-\infty}^{t}dt'\{\dot{z}_1(t')B(t,t',k)+z_1(t')C(t,t',k)+D(t,t',k)[z_1(t')\exp-k^2(t-t')-z_1(t)]\}\ , \tag{11}$$

where $A(t,k)$, $B(t,t',k)$, $C(t,t',k)$, and $D(t,t',k)$ are time-dependent functions determined in Appendix B parameterized by ν the control parameter, K the partition coefficient, and d_0 the capillary length.

Consider first the case of the planar interface moving at constant velocity ($f_0=0$, $z_0=0$). Then, Eq. (11) has a solution of the form $z_1(t)=\Phi\exp(\sigma t)$ where σ satisfies the dispersion relation for disturbances of the planar interface:

$$\left[1-d_0k^2-\frac{1}{2\nu}\right](1+4\sigma+4k^2)^{1/2}=2\sigma+2K\left[d_0k^2+\frac{1}{2\nu}\right]+1-\frac{1}{2\nu}-d_0k^2\ . \tag{12}$$

The corresponding marginal stability curve, the curve $\mathrm{Re}\sigma=0$ in the plane $(k,1/2\nu)$, is drawn in Fig. 3 for $K=0.5$ and $d_0=0.01$, the instable domain lying in the lower part of the diagram.

Numerical integration of Eq. (11) is performed in a similar way as for Eq. (6). In addition, one has previously recorded in a file the steady limit cycle $z_0(t)$ that is used for the computation of the coefficients A, B, C, and D. In order to check the program, one considers the flat nonoscillating steady planar interface ($f_0=0$, $z_0=0$) and verifies that $z_1(t)=\exp\sigma t$ is the solution when Eq. (12) holds between σ and k. Consider the point of coordinates ($k=2.5, 1/2\nu=0.5$) (Fig. 3) lying in the unstable region of the stability diagram obtained for the parameters $K=0.5$ and $d_0=0.01$. Figure 4 shows the evolution of a perturbation of the flat interface oscillating at the frequency $\Omega=2$ for a forcing parameter $f_0=1.5$. The perturbation decays with time so that the parametric oscillation has in this case a stabilizing effect. To evaluate quantitatively the effect one considers the mean value σ of $d\ln|z_1(t)|/dt$. Decay or amplification of a perturbation corresponds to the negative or positive real part of σ. In Table I are reported values of σ for two different sets of parameters. In the first case, $K=0.5$, all the wave numbers considered have negative corresponding values of σ so that the flat oscillating interface can be stabilized in a range of parameters where the flat interface moving at constant velocity is unstable. In the second case $K=0.1$, the interface is not completely stabilized since some wave numbers remain unstable. But the range of unstable wave numbers is reduced.

An analytical expansion at small forcing parameter is necessary in order to understand the stabilizing properties of the parametric oscillation. For this, one uses the multiscale method and expands the perturbation as

$$z_1(t)=Z_0(t,\tau,T)+f_0Z_1(t,\tau,T)+f_0^2Z_2(t,\tau,T)\ , \tag{13}$$

where f_0 is small, $\tau=f_0t$, and $T=f_0t^2$. Solving Eq. (11) up to the second order in f_0, one obtains (see Appendix C)

$$z_1(t)=\Phi_0\exp(\sigma_0t+\sigma_2T)\times\{1+f_0[\lambda_1\exp i\Omega t+\lambda_1^*\exp(-i\Omega t)]\}\ , \tag{14}$$

where λ_1 and σ_2 are determined in Appendix C. Thus, in the limit of small forcing parameter, the growth rate of the perturbation is modified proportionally to the square of this parameter. In Fig. 5, we determine regions where the oscillation has a stabilizing or destabilizing effect.

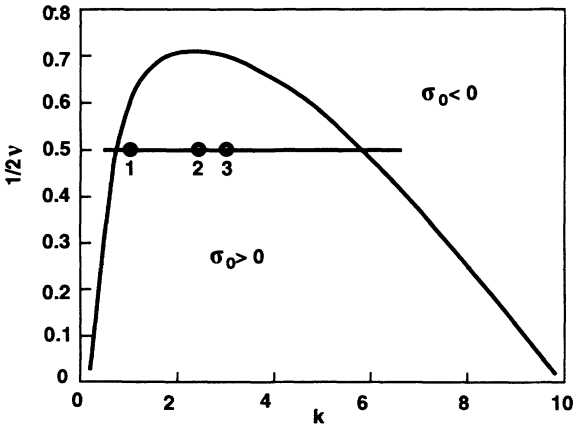

FIG. 3. Marginal stability curve for the flat interface moving at constant velocity. The material parameters are $d_0=0.01$ and $K=0.5$. In the unstable domain three particular points are considered: their wave numbers are, respectively, $k=0.9$, 2.5, and 3.5. They have the same control parameter value $1/2\nu=0.5$.

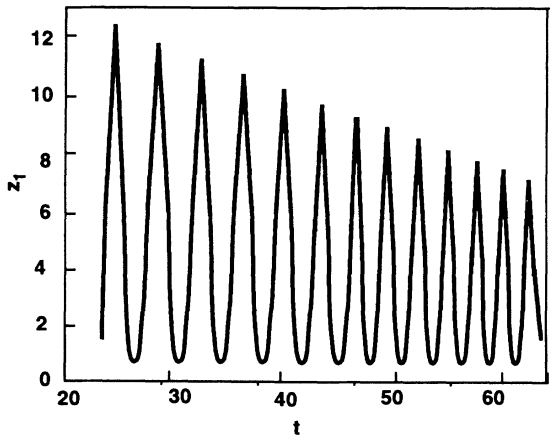

FIG. 4. Time evolution of a perturbation of an oscillatory interface. Here $d_0=0.01$, $K=0.5$, $1/2\nu=0.5$, $\Omega=2$, $f_0=1.5$. The wave number of the perturbation is $k=2.5$.

TABLE I. Values of σ for two different sets of parameters

$d_0=0.01$ $K=0.5$ $\Omega=0.5$, $f_0=4$			$1/2\nu=0.5$ $K=0.1$, $\Omega=1$, $f_0=1.5$		
k	σ_0	σ	k	σ_0	σ
0.9	0.008	−0.45	0.5	0.08	−0.017
2.5	0.67	−0.26	1.7	0.63	0.172
3.5	0.88	−1.2	4.0	1.2	−2.55

Typically [see for instance Fig. 5(a)] the stabilized region $\sigma_2<0$ lies in the center of the diagram, and separates two regions, respectively at small and large wave number, where the oscillation has a destabilizing effect ($\sigma_2>0$). In general, except at very low forcing frequency [Fig. 5(b)], the maximum of the marginal stability curve lies in the stabilized region so that the instability threshold of the oscillating interface occurs at larger pulling velocity than for the flat interface. As can be seen from Figs. 5(a) and 5(b), an increase of the forcing frequency Ω leads to an increase of the size of the stabilized region. From Fig. 6, an increase of the partition coefficient leads to an increase of the size of the stabilized region. The destabilized regions shrinks and eventually disappears for very low frequency [Fig. 6(b)]. Comparison between Figs. 5 and 7 shows that the magnitude of the capillary length is relatively neutral.

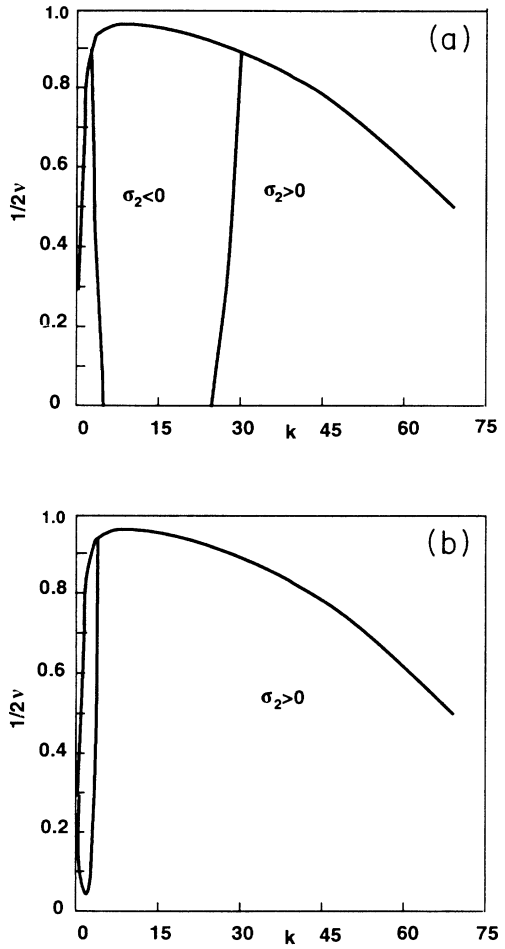

FIG. 5. Regions in the stability diagram where the oscillation has a stabilizing ($\sigma_2<0$) or a destabilizing ($\sigma_2>0$) effect. Here $d_0=0.0001$ and $K=0.15$. In (a), $\Omega=2$, a stabilized region at intermediate wave numbers separates two destabilized regions at low and large wave numbers. In (b), $\Omega=0.05$, the stabilized region shrinks to the benefit of the destabilized region at large wave number. In particular, the marginal wave number of the planar interface moving at constant velocity is now in the destabilized region so that the periodic oscillation favors the morphological instability.

IV. CONCLUSION

We studied the effect of an oscillating growth velocity on the morphological instability of a solidifying liquid

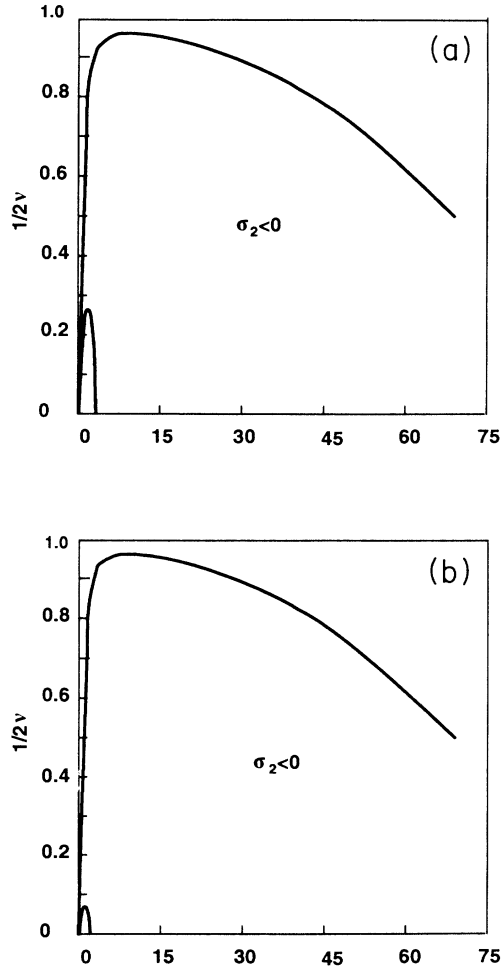

FIG. 6. Regions in the stability diagram where the oscillation has a stabilizing ($\sigma_2<0$) or a destabilizing ($\sigma_2>0$) effect. Here the partition coefficient is larger $K=0.5$, $d_0=0.0001$. In both (a) where $\Omega=2$ and (b) where $\Omega=0.1$, the stabilized region takes the major part of the diagram.

binary mixture. By using an integro-differential equation for the interface we confirm the results of an earlier study by Wheeler [7] that the oscillation of the interface has in general a stabilizing effect on the morphological instability. In addition, we determine, in the small-forcing-parameter limit, the regions in the stability diagram where the oscillation has a stabilizing or a destabilizing effect. A stabilizing effect is found in an intermediate range of wave numbers and for a frequency larger than unity. The stabilizing effect is increased for larger partition coefficient and larger forcing frequencies. The magnitude of the capillary length is relatively neutral concerning this stabilization.

ACKNOWLEDGMENT

The work was performed with the help of Contract No. CNES-PIRMAT 1990.

APPENDIX A: INTEGRO-DIFFERENTIAL EQUATION FOR THE LIQUID-SOLID INTERFACE

We consider the liquid-solid interface as a curve $z(x,t)$ in the frame moving in the z direction with constant unit velocity (we use the same adimensionalizations as in the main text). The corresponding dimensionless diffusion field $u(x,z,t)$ is defined for $z>z(x,t)$. An integro-differential equation for the interface can be determined by using a procedure explained in many papers ([9] for instance) and thus not reproduced here in detail. The analysis starts with the determination of the Green function of the two-dimensional diffusion field, in a frame moving with unity velocity:

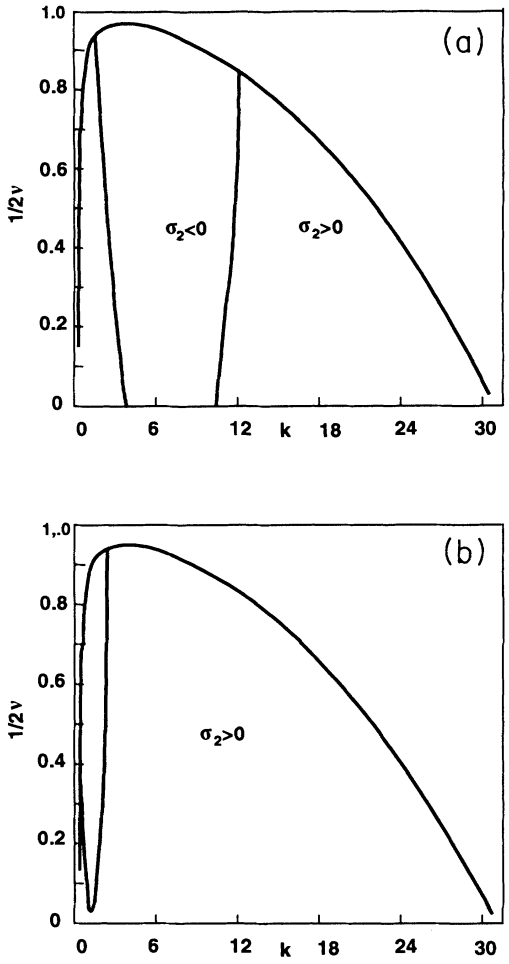

FIG. 7. Regions in the stability diagram where the oscillation has a stabilizing ($\sigma_2<0$) or a destabilizing ($\sigma_2>0$) effect. Here the capillary length is larger $d_0=0.001$, $K=0.15$. If we compare (a) where $\Omega=2$ and (b) where $\Omega=0.1$, respectively, with Figs. 5(a) and (b), we notice that the effect of the capillary length is relatively neutral.

$$G(x,z,t|x',z',t')=\frac{Y(t-t')}{4\pi(t-t')}\exp\left[-\frac{(x-x')^2+(z-z'+t-t')^2}{4(t-t')}\right], \tag{A1}$$

where Y is the Heaviside function. Then the integro-differential equation for the interface is

$$\tfrac{1}{2}u(p)=-\int_{-\infty}^{t}dt'\int_{-\infty}^{+\infty}dx'[1+\dot{z}(x')]u(p')G(p,p')-\int_{-\infty}^{t}dt'\int dl'\mathbf{n}\cdot[G(p,p')\nabla' u(p')-u(p')\nabla' G(p,p')], \tag{A2}$$

where p [p'] is an arbitrary point of the interface of coordinates $(x,z(x))$ [$(x',z(x'))$] and n the unit vector normal to the interface. Here, from Eqs. (2) and (3),

$$u(p)=1-\frac{1}{2\nu}[z(x)-f(t)]-\frac{d_0}{R}, \tag{A3}$$

$$-\frac{\partial u}{\partial n}(p)=\left[1-\frac{(1-K)}{2\nu}[z(x)-f(t)]-\frac{d_0}{R}(1-K)\right][1+\dot{z}(x)]\cos\theta, \tag{A4}$$

where θ is the angle between the normal to the interface and the direction of propagation. Furthermore, the Green function (A1) satisfies the integral relation

$$-\tfrac{1}{2}=-\int_{-\infty}^{t}dt'\int_{-\infty}^{+\infty}dx'[1+\dot{z}(x')]G(p,p')+\int_{-\infty}^{t}dt'\int dl'\mathbf{n}\cdot\nabla' G(p,p') \tag{A5}$$

so that by subtraction of Eq. (A5) from Eq. (A2) and by using boundary conditions (A3) and (A4) one obtains

$$\frac{1}{2}\left[2-\frac{d_0}{R}-\frac{1}{2\nu}[z(x)-f(t)]\right]$$
$$=+\int_{-\infty}^{t}dt'\int_{-\infty}^{+\infty}dx'[1+\dot{z}(x')](1+K)\left[\frac{d_0}{R'}+\frac{1}{2\nu}[z(x')-f(t')]\right]G(p,p')$$
$$-\int_{-\infty}^{t}dt'\int_{-\infty}^{+\infty}dx'\left[\frac{d_0}{R'}+\frac{1}{2\nu}[z(x')-f(t')]\right]\left[\frac{\partial G}{\partial z'}(p,p')-\frac{\partial z}{\partial x'}\frac{\partial G}{\partial x'}(p,p')\right]. \tag{A6}$$

APPENDIX B: INTEGRO-DIFFERENTIAL EQUATION FOR THE LIQUID-SOLID INTERFACE LINEARIZED AROUND THE STEADY STATE $z_0(t)$

Consider a slightly disturbed planar interface $z=z_0(t)+z_1(t)\exp(ikx)$, where z_1 is much smaller than z_0. Then from Eq. (A6), z_1 satisfies

$$\frac{1}{2}\left[-d_0k^2-\frac{1}{2\nu}\right]z_1(t)\exp(ikx)$$
$$=+\int_{-\infty}^{t}dt'\int_{-\infty}^{+\infty}dx'\dot{z}_1(t')\exp(ikx')\left[1+\frac{K}{2\nu}[z_0(t')-f(t')]\right]G(p_0,p_0')$$
$$+\int_{-\infty}^{t}dt'\int_{-\infty}^{+\infty}dx'[1+\dot{z}_0(t')]K\left[d_0k^2+\frac{1}{2\nu}\right]z_1(t')\exp(ikx')G(p_0,p_0')$$
$$+\int_{-\infty}^{t}dt'\int_{-\infty}^{+\infty}dx'[1+\dot{z}_0(t')]\left[1+\frac{K}{2\nu}[z_0(t')-f(t')]\right]$$
$$\times\frac{\partial G}{\partial z}(p_0,p_0')[z_1(t)\exp(ikx)-z_1(t')\exp(ikx')]$$
$$-\int_{-\infty}^{t}dt'\int_{-\infty}^{+\infty}dx'\left[d_0k^2+\frac{1}{2\nu}\right]z_1(t')\exp(ikx')\frac{\partial G}{\partial z'}(p_0,p_0')$$
$$-\int_{-\infty}^{t}dt'\int_{-\infty}^{+\infty}dx'\frac{1}{2\nu}[z_0(t')-f(t')]$$
$$\times\left[-\frac{\partial^2 G}{\partial z^2}(p_0,p_0')[z_1(t)\exp(ikx)-z_1(t')\exp(ikx')]\right.$$
$$\left.-ikz_1(t')\exp(ikx')\frac{\partial G}{\partial x'}(p_0,p_0')\right]. \tag{B1}$$

To proceed further we need to compute the following integrals:

$$\int_{-\infty}^{+\infty}dx'\exp[ik(x'-x)]G(p_0,p_0')=\frac{1}{2\sqrt{\pi}}\frac{1}{(t-t')^{1/2}}\exp\{-[k^2(t-t')]\}\exp\left[-\frac{(z_0-z_0'+t-t')^2}{4(t-t')}\right], \tag{B2}$$

$$\int_{-\infty}^{+\infty}dx'\frac{\partial G}{\partial z}(p_0,p_0')=-\frac{1}{4\sqrt{\pi}}\frac{1}{(t-t')^{3/2}}(z_0-z_0'+t-t')\exp\left[-\frac{(z_0-z_0'+t-t')^2}{4(t-t')}\right], \tag{B3}$$

$$\int_{-\infty}^{+\infty}dx'\exp[ik(x'-x)]\frac{\partial G}{\partial z'}(p_0,p_0')$$
$$=\frac{1}{4\sqrt{\pi}}\frac{1}{(t-t')^{3/2}}(z_0-z_0'+t-t')\exp\{-[k^2(t-t')]\}\exp\left[-\frac{(z_0-z_0'+t-t')^2}{4(t-t')}\right], \tag{B4}$$

$$\int_{-\infty}^{+\infty}dx'\exp[ik(x'-x)]\frac{\partial G}{\partial x'}(p_0,p_0')=\frac{-ik}{2\sqrt{\pi}}\frac{1}{(t-t')^{1/2}}\exp\{-[k^2(t-t')]\}\exp\left[-\frac{(z_0-z_0'+t-t')^2}{4(t-t')}\right], \tag{B5}$$

$$\int_{-\infty}^{+\infty} dx' \exp[ik(x'-x)] \frac{\partial^2 G}{\partial z^2}(p_0,p_0')$$

$$= \left[-\frac{1}{4\sqrt{\pi}} \frac{1}{(t-t')^{3/2}} + \frac{1}{8\sqrt{\pi}} \frac{1}{(t-t')^{5/2}} (z_0 - z_0' + t - t')^2 \right] \exp\{-[k^2(t-t')]\} \exp\left[-\frac{(z_0 - z_0' + t - t')^2}{4(t-t')} \right] , \tag{B6}$$

$$\int_{-\infty}^{+\infty} dx' \frac{\partial^2 G}{\partial z^2}(p_0,p_0')$$

$$= \left[-\frac{1}{4\sqrt{\pi}} \frac{1}{(t-t')^{3/2}} + \frac{1}{8\sqrt{\pi}} \frac{1}{(t-t')^{5/2}} (z_0 - z_0' + t - t')^2 \right] \exp\left[-\frac{(z_0 - z_0' + t - t')^2}{4(t-t')} \right] . \tag{B7}$$

Then the integro-differential equations for $z_1(t)$ can be written as

$$z_1(t) A(t,k) = \int_{-\infty}^{t} dt' \{ \dot{z}_1(t') B(t,t',k) + z_1(t') C(t,t',k) + D(t,t',k) [z_1(t') \exp[-k^2(t-t')] - z_1(t)] \} , \tag{B8}$$

where

$$A(t,k) = \frac{1}{2} \left[-d_0 k^2 - \frac{1}{2\nu} \right] + \int_{-\infty}^{t} dt' \frac{1}{4\sqrt{\pi}} \frac{1}{(t-t')^{1/2}} \exp\left[-\frac{[z_0(t) - z_0'(t') + t - t']^2}{4(t-t')} \right]$$

$$\times \left[[1 + \dot{z}_0(t')] \left[1 + \frac{K}{2\nu} [z_0(t') - f(t')] \right] \frac{1}{(t-t')} [z_0(t) - z_0(t') + t - t'] \right.$$

$$\left. - \frac{1}{4\nu} [z_0(t') - f(t')] \frac{1}{(t-t')^2} [z_0(t) - z_0(t') + t - t']^2 \right] , \tag{B9}$$

$$B(t,t',k) = \frac{1}{2\sqrt{\pi}} \frac{1}{(t-t')^{1/2}} \exp\left[-\frac{[z_0(t) - z_0'(t') + t - t']^2}{4(t-t')} \right] \left[1 + \frac{K}{2\nu} [z_0(t') - f(t')] \right] \exp - [k^2(t-t')] , \tag{B10}$$

$$C(t,t',k) = \frac{1}{4\sqrt{\pi}} \frac{1}{(t-t')^{1/2}} \exp\left[-\frac{[z_0(t) - z_0'(t') + t - t']^2}{4(t-t')} \right] \exp[-k^2(t-t')]$$

$$\times \left[2[1 + \dot{z}_0(t')] K \left[d_0 k^2 + \frac{1}{2\nu} \right] + [1 + \dot{z}_0(t')] \left[1 + \frac{K}{2\nu} [z_0(t') - f(t')] \right] \frac{1}{(t-t')} [z_0(t) - z_0(t') + t - t'] \right.$$

$$- \left[d_0 k^2 + \frac{1}{2\nu} \right] \frac{1}{(t-t')} [z_0(t) - z_0(t') + t - t']$$

$$\left. - \frac{1}{2\nu} [z_0(t') - f(t')] \left[-2k^2 + \frac{1}{2} \frac{1}{(t-t')^2} [z_0(t) - z_0(t') + t - t']^2 \right] \right] , \tag{B11}$$

$$D(t,t',k) = \frac{1}{8\nu\sqrt{\pi}} \frac{[z_0(t') - f(t')]}{(t-t')^{3/2}} \exp\left[-\frac{[z_0(t) - z_0'(t') + t - t']^2}{4(t-t')} \right] . \tag{B12}$$

Here the factor $D(t,t',k)$ was introduced in order to avoid the divergences of the integrals for t' close to t.

APPENDIX C: LINEAR STABILITY ANALYSIS IN THE LIMIT OF SMALL FORCING PARAMETER

Assume that the forcing parameter f_0 is small so that the unperturbed solution $z_0(t)$ is determined by Eq. (8). Introduce the time scales $t, \tau = f_0 t$, and $T = f_0^2 t$, and as is usual for a standard multiscale method, expand the solution of Eq. (12) as

$$z_1(t) = Z_0(t,\tau,T) + f_0 Z_1(t,\tau,T) + f_0^2 Z_2(t,\tau,T) . \tag{C1}$$

Furthermore, expand the coefficients $A(t,k)$, $B(t,t',k)$, $C(t,t',k)$, and $D(t,t',k)$ as

$$A(k) = A_0(k) + f_0 (A_1(k) \exp(i\Omega t) + A_1^*(k) \exp(-i\Omega t)) + f_0^2 (A_{20}(k) + A_{22}(k) \exp(2i\Omega t) + A_{22}^*(k) \exp(-2i\Omega t)) , \tag{C2}$$

$$B(t,t',k)=B_0(t,t',k)+f_0(B_1(t,t',k)\exp(i\Omega t)+B_1^*(t,t',k)\exp(-i\Omega t))$$
$$+f_0^2(B_{20}(t,t',k)+B_{22}(t,t',k)\exp(2i\Omega t)+B_{22}^*(t,t',k)\exp(-2i\Omega t)) , \tag{C3}$$
$$C(t,t',k)=C_0(t,t',k)+f_0(C_1(t,t',k)\exp(i\Omega t)+C_1^*(t,t',k)\exp(-i\Omega t))$$
$$+f_0^2(C_{20}(t,t',k)+C_{22}(t,t',k)\exp(2i\Omega t)+C_{22}^*(t,t',k)\exp(-2i\Omega t)) , \tag{C4}$$
$$D(t,t',k)=f_0(D_1(t,t',k)\exp(i\Omega t)+D_1^*(t,t',k)\exp(-i\Omega t))$$
$$+f_0^2(D_{20}(t,t',k)+D_{22}(t,t',k)\exp(2i\Omega t)+D_{22}^*(t,t',k)\exp(-2i\Omega t)) , \tag{C5}$$

where all the coefficients are determined in Appendix D.

At zeroth order of the expansion, one obtains

$$Z_0(t)A_0(k)=\int_{-\infty}^{t}dt'[\dot{Z}_0(t')B_0(t,t',k)+Z_0(t')C_0(t,t',k)] . \tag{C6}$$

Introduce now the quantities

$$\beta_n(q,k)=\int_{-\infty}^{t}dt'\exp[-q(t-t')]B_n(t,t',k) , \tag{C7}$$
$$\gamma_n(q,k)=\int_{-\infty}^{t}dt'\exp[-q(t-t')]C_n(t,t',k) , \tag{C8}$$

for $n=0,1,2$. The solution of Eq. (C6) can be found as $Z_0(t)=\Phi_0(\tau,T)\exp[\sigma_0(k)t]$ where $\sigma_0(k)$ is the Mullins-Sekerka growth rate solution of Eq. (12) or in the more concise form

$$\Delta(\sigma_0,k)=A_0(k)-\sigma_0\beta_0(\sigma_0,k)-\gamma_0(\sigma_0,k)=0 . \tag{C9}$$

At the following order of the expansion, one obtains:

$$Z_1(t)A_0(k)-\int_{-\infty}^{t}dt'[\dot{Z}_1(t')B_0(t,t',k)+Z_1(t')C_0(t,t',k)]$$
$$=-Z_0(t)A_1(k)+\int_{-\infty}^{t}dt'(Z_0(t')[B_1(t,t',k)\exp(i\Omega t)+B_1^*(t,t',k)\exp(-i\Omega t)]$$
$$+Z_0(t')[C_1(t,t',k)\exp(i\Omega t)+C_1^*(t,t',k)\exp(-i\Omega t)]+\frac{d\Phi}{d\tau}B_0(t,t',k)\exp\sigma_0 t'$$
$$+\{Z_0(t')\exp[-k^2(t-t')]-Z_0(t)\}[D_1(t,t',k)\exp(i\Omega t)+D_1^*(t,t',k)\exp(-i\Omega t)]) . \tag{C10}$$

Introduce the quantity

$$\delta_n(q,k)=\int_{-\infty}^{t}dt'\exp[-(q+k^2)(t-t')-1]D_n(t,t',k) . \tag{C11}$$

Then, the solution of Eq. (C10) can be found as

$$Z_1(t,\tau,T)=\Phi_1(\tau,T)\exp(\sigma_0 t+i\Omega t)+\Phi_1^*(\tau,T)\exp(\sigma_0 t-i\Omega t)+\phi_1\frac{d\Phi_0}{d\tau}t\exp(\sigma_0 t) , \tag{C12}$$

where

$$\Phi_1(\tau,T)=\lambda_1\Phi_0(\tau,T) , \quad \lambda_1=\frac{1}{\Delta(\sigma_0+i\Omega,k)}[-A_1+\sigma_0\beta_1(\sigma_0,k)+\gamma_1(\sigma_0,k)+\delta_1(\sigma_0,k)] , \tag{C13}$$

and

$$\phi_1\frac{1+4k^2+4\sigma_0}{(2K-1)\left[d_0k^2+\frac{1}{2\nu}\right]-2\sigma_0-4k^2} . \tag{C14}$$

As usual in a multiscale method, the first correction f_0Z_1 must be much smaller than the main term Z_0 up to a time of order $1/f_0$. This is the case if the last term of the rhs of the equation vanishes (secular term), i.e., if $d\Phi/d\tau=0$.

At the second order of the expansion, one obtains

$$
\begin{aligned}
&Z_2(t)A_0(k)-\int_{-\infty}^{t}dt'[\dot{Z}_2(t')B_0(t,t',k)+Z_2(t')C_0(t,t',k)] \\
&\quad=-Z_0(t)[A_{20}(k)+A_{22}(k)\exp(2i\Omega t)+A_{22}^{*}(k)\exp(-2i\Omega t)]-Z_1(t)[A_1(k)\exp(i\Omega t)+A_1^{*}(k)\exp(-i\Omega t)] \\
&\quad+\int_{-\infty}^{t}dt'\Big[\dot{Z}_0(t')[B_{20}(t,t',k)+B_{22}(t,t',k)\exp(i\Omega t)+B_{22}^{*}(t,t',k)\exp(-2i\Omega t)] \\
&\qquad+\int_{-\infty}^{t}dt'(\dot{Z}_1(t')[B_1(t,t',k)\exp(i\Omega t)+B_1^{*}(t,t',k)\exp(-i\Omega t)] \\
&\qquad+\int_{-\infty}^{t}dt'\frac{d\Phi}{dT}B_0(t,t',k)\exp\sigma_0 t' \\
&\qquad+\int_{-\infty}^{t}dt'Z_0(t')[C_{20}(t,t',k)+C_{22}(t,t',k)\exp(2i\Omega t)+C_{22}^{*}(t,t',k)\exp(-2i\Omega t)] \\
&\qquad+\int_{-\infty}^{t}dt'\Big[Z_1(t')[C_1(t,t',k)\exp(i\Omega t)+C_1^{*}(t,t',k)\exp(-i\Omega t)] \\
&\qquad\qquad+\int_{-\infty}^{t}dt'Z_0(t')\exp[-k^2(t-t')]-Z_0(t) \\
&\qquad\qquad\times[D_{20}(t,t',k)+D_{22}(t,t',k)\exp(2i\Omega t)+D_{22}^{*}(t,t',k)\exp(-2i\Omega t)]\Big] \\
&\qquad\qquad+\int_{-\infty}^{t}dt'\{Z_1(t')\exp[-k^2(t-t')]-Z_1(t)\}[D_1(t,t',k)\exp(i\Omega t) \\
&\qquad\qquad\qquad+D_1^{*}(t,t',k)\exp(-i\Omega t)])\Big] .
\end{aligned}
\tag{C15}
$$

As in the case of the first order of the expansion, one collects all the secular terms [proportional to $\exp(\sigma_0 t)$] of the rhs of Eq. (C15) and obtains

$$
\begin{aligned}
\frac{d\Phi_0}{dT}=\frac{\Phi_0(T)}{\beta_0(\sigma_0,k)}&[A_{20}(k)-\sigma_0\beta_{20}(\sigma_0,k)-\gamma_{20}(\sigma_0,k)-\delta_{20}(\sigma_0,k)+A_1\lambda_1^{*}+A_1^{*}\lambda_1-(\sigma_0-i\Omega)\beta_1(\sigma_0-i\Omega,k)\lambda_1^{*} \\
&-(\sigma_0+i\Omega)\beta_1^{*}(\sigma_0+i\Omega,k)\lambda_1-\gamma_1(\sigma_0-i\Omega,k)\lambda_1^{*}-\gamma_1^{*}(\sigma_0+i\Omega,k)\lambda_1-\delta_1(\sigma_0-i\Omega,k)\lambda_1^{*} \\
&-\delta_1^{*}(\sigma_0+i\Omega,k)\lambda_1] .
\end{aligned}
\tag{C16}
$$

Thus the Mullins-Sekerka growth rate σ_0 is modified by the parametric forcing as $\sigma=\sigma_0+f_0^2\sigma_2$ where σ_2 is determined as

$$
\begin{aligned}
\sigma_2=\frac{1}{\beta_0(\sigma_0,k)}&[A_{20}(k)-\sigma_0\beta_{20}(\sigma_0,k)-\gamma_{20}(\sigma_0,k)-\delta_{20}(\sigma_0,k)+A_1\lambda_1^{*}+A_1^{*}\lambda_1 \\
&-(\sigma_0-i\Omega)\beta_1(\sigma_0-i\Omega,k)\lambda_1^{*}-(\sigma_0+i\Omega)\beta_1^{*}(\sigma_0+i\Omega,k)\lambda_1-\gamma_1(\sigma_0-i\Omega,k)\lambda_1^{*} \\
&-\gamma_1^{*}(\sigma_0+i\Omega,k)\lambda_1-\delta_1(\sigma_0-i\Omega,k)\lambda_1^{*}-\delta_1^{*}(\sigma_0+i\Omega,k)\lambda_1] .
\end{aligned}
\tag{C17}
$$

APPENDIX D: COEFFICIENTS USED FOR THE LINEAR STABILITY ANALYSIS

$$
A_0(k)=\frac{1}{2}\left[1-d_0k^2-\frac{1}{2\nu}\right] ,
\tag{D1}
$$

$$
\beta_0(q,k)=\frac{1}{(1+4k^2+4q)^{1/2}}
\tag{D2}
$$

$$
\gamma_0(q,k)=\tfrac{1}{2}\left[1+(2K-1)\left[d_0k^2+\frac{1}{2\nu}\right]\right]\frac{1}{(1+4k^2+4q)^{1/2}} ,
\tag{D3}
$$

$$
A_1=-\frac{\alpha_1}{8i}(2-\sqrt{1+4i\Omega})+\frac{1}{\sqrt{1+4i\Omega}}\left[\frac{\alpha_1(1+2i\Omega)}{8i}+\frac{(2K-1)}{16i\nu}(\alpha_1-1)\right] ,
\tag{D4}
$$

$$\beta_1(q,k)=-\frac{1}{4i}\alpha_1\frac{1}{(1+4k^2+4q)^{1/2}}+\frac{1}{[1+4k^2+4(q+i\Omega)]^{1/2}}\left[\frac{1}{4i}\left[\frac{K}{\nu}(\alpha_1-1)+\alpha_1\right]\right], \tag{D5}$$

$$\begin{aligned}\gamma_1(q,k)=&-\frac{1}{4i}\alpha_1\frac{1}{[1+4(k^2+q)]^{1/2}}\left[\frac{2K-1}{2}\left[d_0k^2+\frac{1}{2\nu}\right]+\frac{1}{2}\right]\\&+\frac{1}{8i}\alpha_1\{[1+4(k^2+q)+4i\Omega]^{1/2}-[1+4(k^2+q]^{1/2}\}\left[1-\left[d_0k^2+\frac{1}{2\nu}\right]\right]\\&+\frac{1}{[1+4(k^2+q)+4i\Omega]^{1/2}}\left\{\frac{1}{2\nu}\frac{1}{4i}\left[\frac{2K-1}{2}+2k^2\right](\alpha_1-1)\right.\\&\left.+\frac{\alpha_1\Omega}{2}\left[K\left[d_0k^2+\frac{1}{2\nu}\right]+\frac{1}{2}\right]+\frac{\alpha_1}{8i}\left[(2K-1)\left[d_0k^2+\frac{1}{2\nu}\right]+1\right]\right\},\end{aligned} \tag{D6}$$

$$\delta_1(q,k)=\frac{1}{16\nu i}(\alpha_1-1)\{\sqrt{1+4i\Omega}-[1+4i\Omega+4(k^2+9)]^{1/2}\}, \tag{D7}$$

$$\begin{aligned}A_{20}=&\frac{2K-1}{32\nu}\beta_2+|\alpha_1|^2\frac{\Omega}{8}\left[\mathrm{Im}\frac{1}{\sqrt{1+4i\Omega}}+\mathrm{Im}\sqrt{1+4i\Omega}\right]+|\alpha_1|^2\left[\tfrac{1}{4}-\tfrac{3}{16}\mathrm{Re}\sqrt{1+4i\Omega}-\tfrac{1}{16}\mathrm{Re}\frac{1}{\sqrt{1+4i\Omega}}\right]\\&+\frac{K}{8\nu}\Omega\,\mathrm{Im}\alpha_1+\mathrm{Re}\alpha_1^*(\alpha_1-1)\left[\frac{4K-3}{32\nu}-\frac{(K-1)}{16\nu}\sqrt{1+4i\Omega}-\frac{(2K-1)}{32\nu}\frac{1}{\sqrt{1+4i\Omega}}\right],\end{aligned} \tag{D8}$$

$$\begin{aligned}\beta_{20}(1,k)=&\frac{K}{8\nu}\frac{1}{[1+4(k^2+q)]^{1/2}}\beta_2+|\alpha_1|^2\left[\frac{1}{8}\left[\frac{1}{[1+4(k^2+q)]^{1/2}}-\mathrm{Re}\frac{1}{[1+4(k^2+q)+4i\Omega]^{1/2}}\right]\right.\\&\left.+\frac{1}{8}[1+4(k^2+q)]^{1/2}-\mathrm{Re}[1+4(k^2+q)+4i\Omega)]^{1/2}\right]\\&+\mathrm{Re}\alpha_1^*(\alpha_1-1)\frac{K}{8\nu}\left[\frac{1}{[1+4(k^2+q)]^{1/2}}-\frac{1}{[1+4(k^2+q)+4i\Omega]^{1/2}}\right],\end{aligned} \tag{D9}$$

$$\begin{aligned}\gamma_{20}(q,k)=&\frac{2K+4k^2-1}{32\nu}\frac{1}{[1+4(k^2+q)]^{1/2}}\beta_2\\&+|\alpha_1|^2\frac{\Omega}{8}\left[1+2K\left[d_0k^2+\frac{1}{2\nu}\right]\right]\left[\mathrm{Im}\frac{1}{[1+4(k^2+q)+4i\Omega]^{1/2}}+\mathrm{Im}[1+4(k^2+q)+4i\Omega)]^{1/2}\right]\\&+|\alpha_1|^2\frac{1}{16}\left[1+(2K-1)\left[d_0k^2+\frac{1}{2\nu}\right]\right]\left[\frac{1}{[1+4(k^2+q)]^{1/2}}-\mathrm{Re}\frac{1}{[1+4(k^2+q)+4i\Omega]^{1/2}}\right]\\&+\frac{1}{16}\left[3+(2K-3)\left[d_0k^2+\frac{1}{2\nu}\right]\right]\{[1+4(k^2+q)]^{1/2}-\mathrm{Re}[1+4(k^2+q)+4i\Omega]^{1/2}\}\\&+\frac{K}{8\nu}\Omega\,\mathrm{Im}\alpha_1\frac{1}{[1+4(k^2+q)]^{1/2}}\\&+\mathrm{Re}\alpha_1^*(\alpha_1-1)\frac{(2K-1+4k^2)}{32\nu}\left[\frac{1}{[1+4(k^2+q)]^{1/2}}-\frac{1}{[1+4(k^2+q)+4i\Omega]^{1/2}}\right]\\&+\frac{K-1}{16\nu}\{1+4(k^2+q)]^{1/2}-[1+4(k^2+q)+4i\Omega]^{1/2}\},\end{aligned} \tag{D10}$$

$$\begin{aligned}\delta_{20}(q,k)=&\frac{\beta_2}{32\nu}\{1-[1+4(k^2+q)]^{1/2}\}+\frac{1}{32\nu}\mathrm{Re}\alpha_1^*(\alpha_1-1)([1+4(k^2+q)+4i\Omega]^{1/2}-[1+4i\Omega]^{1/2}+1\\&-[1+4(k^2+q)]^{1/2}).\end{aligned} \tag{D11}$$

[1] W. Kurz and D. J. Fisher, *Fundamentals of Solidification,* 3rd ed. (Trans Tech, Aedermannsdorf, Switzerland, 1989).
[2] M. A. Eshelman, V. Seetharaman, and R. Trivedi, Acta Metall. **36**, 1165 (1988).
[3] P. Kurowski, C. Guthmann, and S. de Cheveigne, Phys. Rev. A **42**, 7368 (1990).
[4] G. Searby, Combust. Sci. Technol. **81**, 221 (1992).
[5] G. H. Markstein, *Nonsteady Flame Propagation* (Pergamon, New York, 1964).
[6] G. Searby and D. Rochwerger, J. Fluid, Mech. **231**, 529 (1991).
[7] A. A. Wheeler, J. Cryst. Growth **67**, 8 (1984).
[8] D. Rochwerger, Ph.D. thesis, Université de Provence, Marseille, 1991.
[9] B. Caroli, C. Caroli, B. Roulet, and J. S. Langer, Phys. Rev. A **33**, 442 (1986).